Journal of Industrial and Engineering Chemistry xxx (2015) xxx–xxx

Contents lists available at ScienceDirect

Journal of Industrial and Engineering Chemistry

journal homepage: www.elsevier.com/locate/jiec

Oxidative steam reforming of isobutanol over Ni/γ-Al_2O_3 catalysts: A comparison with thermodynamic equilibrium analysis

Q1 Vimala Dhanala, Sunil K. Maity *, Debaprasad Shee

Department of Chemical Engineering, Indian Institute of Technology Hyderabad, Ordnance Factory Estate, Yeddumailaram 502205, Telangana, India

ARTICLE INFO

Article history:
Received 15 September 2014
Received in revised form 30 November 2014
Accepted 7 December 2014
Available online xxx

Keywords:
Oxidative steam reforming
Thermodynamic equilibrium analysis
Bio-butanol
Synthesis gas
Ni/γ-Al_2O_3
Q2 Spent catalyst

ABSTRACT

Present work provides a systematic investigation of oxidative steam reforming (OSR) and comparisons with steam reforming (SR) of isobutanol over γ-Al_2O_3 supported nickel catalysts. Catalysts characterization results demonstrated that majority of nickel oxide was present as dispersed $NiAl_2O_4$. The hydrogen yield and selectivity to CO and methane were somewhat lesser for OSR compared to SR. The H_2/CO mole ratio in the range of 8–10 was observed under the experimental conditions. The experimental results were matched well with equilibrium products compositions. The spent catalysts were further characterized to elucidate chemical and morphological changes of the catalysts during SR and OSR.

Introduction

Q3 Synthesis gas (SG) is a key petrochemical building block chemical for manufacture of extensive ranges of fuels and organic chemicals. It is mainly used as raw material for manufacture of hydrogen, ammonia, fertilizers, methanol, and dimethyl ether. SG also provides a source of highly pure hydrogen for fuel cell applications to generate electric power in an environmentally cleaner manner. SG is generally produced by steam reforming (SR) of fossil fuels derived hydrocarbons such as naphtha and natural gas. The fossil fuels are however diminishing relentlessly to meet growing demands of energy and organic chemicals. Moreover, concentration of toxic and greenhouse gases is rising steadily in earth atmosphere due to large scale usage of fossil fuels. Therefore, shifting dependency away from finite fossil fuels to carbon-neutral renewable resources like biomass is highly essential for sustainability of human civilization as a whole while maintaining environmental cleanliness. The biomass being origin of fossil fuels has remarkable potential in principle to deliver societal needs of transportation fuels, energy (heat and electricity), and organic chemicals. Therefore, new manufacturing concepts are continuously emerging for manufacture of assembly of bio-fuels and organic chemicals from biomass using complex processing technologies similar to today's integrated petroleum refinery and petrochemical industries commonly known as biorefinery [1,2].

The gasification is a potential thermochemical process for direct conversion of lignocellulosic biomass into SG. However, excessive formation of tars and methane, gigantic size of plant with huge capital investments, and non-concentric nature of biomass make integrated technology of biomass gasification and biomass-to-liquid economically impractical [3]. The reforming of biomass derived oxygenated compounds including bio-oils, ethanol, and butanols are another promising approach for production of SG [4–6]. In recent times, bio-butanols (n- and iso-) have attracted renewed attention worldwide as a promising forthcoming bio-fuel because of its superior fuel qualities [7,8]. The favourable features enable direct applications of butanols in existing internal combustion engines without any engine modifications. Moreover, butanols have wide range of potentials as solvent, derivatives, and petrochemical feedstocks to fulfil goals of integrated biorefinery [2,9]. Once bio-butanols based biorefinery is realized successfully, novel methods of production of hydrogen and SG must also be established from bio-butanols.

Abbreviations: CCGP, carbon conversion to gaseous products, %; d_c, crystallite size, nm; FBR, fixed-bed reactor; OCMR, oxygen-to-carbon mole ratio; OSR, oxidative steam reforming; PV, pore volume, cm^3/gm; SA, BET surface area, m^2/g; SCMR, steam-to-carbon mole ratio; SG, synthesis gas; SR, steam reforming; WGSR, water-gas shift reaction; WHSV, weight hourly space velocity, h^{-1}.

* Corresponding author. Tel.: +91 40 2301 6075; fax: +91 40 2301 6003.
E-mail address: sunil_maity@iith.ac.in (S.K. Maity).

http://dx.doi.org/10.1016/j.jiec.2014.12.029
1226-086X/

SR and partial oxidation (PO) are two possible approaches for production of SG from butanols. SR is however accompanied with external supply of huge quantities heat energy to supplement endothermic reactions. The problem of external heat supply can be circumvented by exothermic PO of butanols. The technology of PO however suffers from drawbacks of low hydrogen yield and H_2/CO mole ratio compared to SR. The oxidative steam reforming (OSR) using sub-stoichiometric level of oxygen is an attractive alternative where exothermic PO reactions provide necessary heat energy for endothermic SR reactions. Moreover, SG obtained from OSR can be used either directly in high temperature fuel cell such as SOFC or in PEM fuel cell for mobile applications after significant reduction of CO level below 10 ppm (by membrane coupled reformer or WGS reactor followed by a COPROX reactor) to overcome poisoning of Pt catalyst [10]. Apprehending tremendous upcoming prospective of bio-butanols based biorefinery, present work was initiated on OSR of isobutanol for production of SG.

Despite having enormous potential, only a few experimental studies are available in public domain on SR and PO of butanols and ABE solvents mixture over Al_2O_3, CeO_2, ZnO, and TiO_2 supported nickel and cobalt catalysts modified by copper, magnesium, iridium, and rhodium [11–15]. The Ni/CeO_2 demonstrated superior catalytic activity over Ni/Al_2O_3 due to oxygen mobility characteristics of CeO_2 [14]. Co-precipitated Ni/Al_2O_3 modified by copper showed enhanced catalyst stability with concurrent reduction of catalytic activity [11]. Co/ZnO exhibited higher catalytic activity over Co/TiO_2 and Co/CeO_2 and addition of iridium increased hydrogen yield and decreased selectivity to CH_4 [12].

The experimental studies on OSR of butanols are also limited in open literatures. Autothermal reforming of isobutanol was first reported over α-Al_2O_3 supported 1 wt%Rh–1 wt%Ce catalyst in a stagedmillisecond contact reactor [16]. Addition of 1 wt%Pt–1 wt%Ce in the downstream of reformer improved purity of hydrogen with H_2/CO mole ratio of 12 and selectivity to CO of 1.7–3 mol% at SCR of 2 or 3. Recently, OSR of ABE solvents mixture was extensively studied over ZnO, TiO_2, and CeO_2–ZrO_2 supported cobalt and cobalt–iridium catalysts promoted by different noble metals (ruthenium, rhodium, iridium, and palladium) [17–20]. The bimetallic catalyst exhibited enhanced catalytic activity with lesser catalyst deactivation than monometallic catalysts. Rhodium promoted cobalt exhibited highest catalytic activity among tested promoters.

Thermodynamic equilibrium analysis is a valuable tool to foresee viability of process, effects of process parameters on equilibrium products composition, and thermodynamically favourable and optimum operating conditions of the process. Apprehending importance, numerous studies have also been dedicated in the past exclusively on thermodynamic equilibrium analysis of SR, PO, OSR, sorption enhanced SR, and dry reforming of butanols [13,21–25]. From the above discussion, it is quite evident that comparison of experimental OSR results with SR of isobutanol over γ-Al_2O_3 supported nickel catalysts and validation with equilibrium composition has not been reported so far. The present work was therefore undertaken to authenticate experimental SR and OSR data with thermodynamics equilibrium analysis results. Elucidation of chemical and morphological changes of the catalysts during SR and OSR is another objective of this work.

Methodology

Catalysts preparation and characterization

γ-Al_2O_3 (Alfa Aesar) supported nickel catalysts were prepared by incipient wetness impregnation method using nickel nitrate hexahydrate ($Ni(NO_3)_2{\cdot}6H_2O$, ≥97%, Merck India Ltd., Mumbai) as precursor. Requisite amounts of nickel precursor were first dissolved in distilled water of volume equal to (or slight excess of) pore volume of γ-Al_2O_3. γ-Al_2O_3 pellets were then immersed into precursor solution with continuous stirring for one hour for uniform distribution of precursor over entire surface of the support. The wet materials were finally dried overnight at 353 K followed by calcination at 923 K. The calcined γ-Al_2O_3 supported nickel oxide catalysts with 20 and 30 wt% nickel loading were abbreviated as 20NiOAl and 30NiOAl respectively throughout the article. The reduced (at 923 K using hydrogen) 20NiOAl and 30NiOAl were designated as 20NiAl and 30NiAl respectively.

BET surface area (SA) and pore volume (PV) of the catalysts were measured using Micromeritics ASAP 2020 physisorption analyser. SAs were calculated from adsorption isotherm data at 77 K using multipoint BET equation. The volume of liquid nitrogen adsorbed at P/P_0 = ca.1.0 was considered as PV. Powder XRD patterns of the catalysts were measured by Phillips X-pert diffractometer using CuKα radiation (λ = 1.541 Å, 30 kV) at a 2θ interval of 10–100° with a scanning speed of 0.09°/s. The metal/metal oxide crystallite sizes were calculated for different planes by Scherrer's equation using full width half maximum of the XRD peaks. Hydrogen pulse chemisorption and temperature programmed reduction (TPR) studies were performed in Micromeritics AutoChem II 2920 chemisorption analyser using 10 vol% H_2–Ar gas mixture. Metal dispersion (MD) and active metal surface area (SM) of the catalysts were calculated based on amounts of chemisorbed hydrogen considering surface stoichiometry as H_2/Ni = 0.5. The temperature corresponding to maximum hydrogen consumption was considered as maximum reduction temperature (T_{max}). Field emission gun scanning electron microscopy (FESEM) images of spent catalysts were captured using Zeiss Supra 40 equipped with energy dispersive X-ray detector (EDX). The elemental compositions of spent catalysts were determined using EDX analysis over a selected surface.

Experimental setup and procedure

SR and OSR of isobutanol were carried out in a computer controlled down-flow fixed-bed reactor equipped with two mass flow controllers (MFC) and two HPLC pumps in the upstream and a condenser and a wet gas metre in the downstream. Details of experimental setup can be found elsewhere [13]. For a typical experiment, about 3 g of calcined catalyst pellets was mixed with about 15 g of similar size quartz beads and the mixture was loaded into the reactor. The catalysts bed was supported by layers of quartz wools from both sides. The reactor was then embedded inside a vertical tubular furnace consisting of two heating zones (preheating and reaction). The temperature of the reaction zone was controlled by a PID controller within ±1 K. The calcined catalysts were first reduced at 923 K using pure hydrogen with a flow rate of 20 ml/min for about 3 h. Isobutanol and water were pumped using two separate HPLC pumps to pre-heater (maintained at 523 K) where feed was vaporized before entering into the reactor. Controlled volume of nitrogen (53.3 ml/min) and oxygen was introduced into the reactor using individual MFCs through an intermediate pre-heater. Nitrogen was used as carrier gas as well as internal standard of the reaction for calibration of gaseous products. The exit stream from reactor was passed through a vertical condenser (maintained at 270 K) to allow condensation of volatile compounds. The cumulative volumetric flow rate of non-condensable gases leaving the condenser was recorded with time-on-stream (TOS) using a wet gas metre. The condensed liquids were also collected time-to-time from condenser to check consistency in material balance. Material balance was checked under steady state for all experiments and errors were obtained within ±5%. The compositions of gaseous products were measured by online gas chromatography (Shimazdu GC 2014) using TCD. The oxygenated compounds of condensed liquid were identified by offline GC equipped with mass spectrometer (MS) detector (Shimazdu GC 2010) using helium as carrier gas and quantified by GC

Please cite this article in press as: V. Dhanala, et al., J. Ind. Eng. Chem. (2015), http://dx.doi.org/10.1016/j.jiec.2014.12.029

equipped with FID using ZB wax capillary column (30 m × 0.25 mm × 0.25 μm). The products of condensed liquid were also calibrated using HPLC grade pure compounds.

Thermodynamic equilibrium analysis

Thermodynamic equilibrium analysis of SR and OSR of isobutanol was carried out using equilibrium reactor model (R-Gibbs) available in Aspen Plus®, Aspen Tech™ software. The R-Gibbs reactor model calculates equilibrium products composition based on the principle of minimization of Gibbs free energy of the whole system considering all components as product. The thermodynamic equilibrium analysis was performed considering feed consisting of isobutanol, water, and oxygen entered into R-Gibbs reactor at the temperature of reactor. In the present study, hydrogen, carbon monoxide, carbon dioxide, methane, and oxygen (in case of OSR) together with carbon (graphite) and various hydrocarbons and oxygenated hydrocarbons with four or less carbon atoms were considered as probable products in both SR and OSR. The equilibrium mole fraction of carbon (graphite), compounds containing two or more carbon atoms, and oxygen (in case of OSR) was however negligibly small for the whole range of process conditions examined. Hence these products were not considered for subsequent studies. Complete conversion of isobutanol was observed throughout the thermodynamic equilibrium analysis. The algorithm of thermodynamic equilibrium analysis was elaborated in our earlier publications [26,27].

Results and discussion

Catalyst characterization

The physicochemical properties of the catalysts are presented in Table 1. Pure γ-Al_2O_3 (calcined at 923 K) has SA and PV of 228 m^2/g and 0.84 cm^3/g respectively. The SA and PV of γ-Al_2O_3 supported calcined (20NiOAl and 30NiOAl) and reduced (20NiAl and 30NiAl) nickel catalysts were significantly lesser than pure γ-Al_2O_3 due to coverage of γ-Al_2O_3 surface by nickel/nickel oxide crystallites or blockage of pore mouths.

The powder XRD patterns of both calcined and reduced catalysts are shown in Fig. 1. The powder XRD patterns of calcined γ-Al_2O_3 and bulk nickel oxide were also acquired for clear discrimination of nickel peaks from support and nickel oxide peaks. The bulk nickel oxide peaks were appeared at 2θ of 37.3° (1 1 1) and 43.2° (2 0 0) for calcined catalysts [PDF#750197]. The peaks observed at 2θ of 37.3° (3 1 1) and 66.2° (4 4 0) were attributed to differently coordinated dispersed nickel-aluminate ($NiAl_2O_4$) [PDF#780552].

Table 1
Physicochemical properties of the catalysts.

Catalysts	SA	PV	MD	SM	d_c	T_{max} (K)
γ-Al_2O_3	228	0.84	–	–	–	–
20NiOAl	178	0.6	–	–	12.8*	745, 988
30NiOAl	137	0.47	–	–	18.8*	782, 1000
20NiAl[a]	166	0.6	1.86	12.4	11.8**	–
30NiAl[b]	109	0.43	1.73	11.5	18.6**	–

SA, BET surface area, m^2/g; PV, pore volume, cm^3/g; MD, metal dispersion, %; SM, metallic surface area, m^2/g metal; d_c, average nickel**/nickel oxide* crystallite size, nm.

[a] For spent catalysts: average nickel crystallite sizes were 15.3, 14.2, and 8.2 nm and nickel oxide crystallite sizes were 7.3, 8.4, 8.1, and 8.7 nm for OCMR of 0, 0.8, 1.7, and 2.5 respectively. Reaction conditions: 873 K, SCMR = 2.5, WHSV = 7.02–8.9 h^{-1}.

[b] For spent catalysts: average nickel crystallite sizes were 22.6 and 22.1 nm and nickel oxide crystallite sizes were 6.9 and 7.8 nm for OCMR of 0 and 0.8 respectively. Reaction conditions: 923 K, SCMR = 2.5, WHSV = 7.6 h^{-1}.

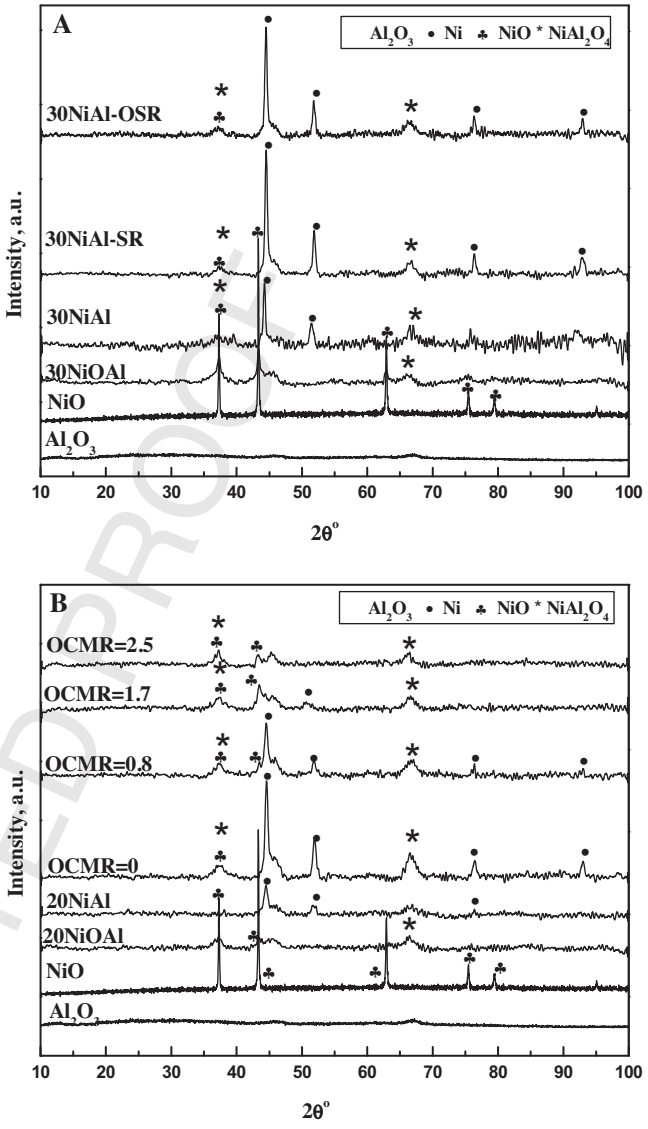

Fig. 1. Powder XRD patterns of (A) γ-Al_2O_3, NiO, 30NiOAl, 30NiAl, and spent 30NiAl and (B) γ-Al_2O_3, NiO, 20NiOAl, 20NiAl, and spent 20NiAl catalysts. Conditions: 923 K, SCMR = 2.5, WHSV = 7.02 h^{-1} (SR) and 7.6 h^{-1}(OSR), OCMR = 0.8 (30NiAl).

The powder XRD patterns of 20NiAl showed only characteristic nickel peaks indicating that nickel oxides of 20NiOAl were completely converted to metallic nickel during reduction at 923 K. The powder XRD patterns of 30NiAl however exhibited additional $NiAl_2O_4$ peaks due to incomplete reduction of $NiAl_2O_4$. The characteristic nickel peaks were identified at 2θ of 44.44° (1 1 1), 51.5° (2 0 0), and 76.4° (2 2 0) for both 20NiAl and 30NiAl (PDF#650380). As observed from Fig. 1, nickel/nickel oxide crystallites were enlarged with increasing nickel loading on γ-Al_2O_3 due to agglomeration of nickel/nickel oxide at higher nickel loadings on γ-Al_2O_3. The agglomeration of nickel/nickel oxide also caused decrease of MD and SM with increasing nickel loadings on γ-Al_2O_3 (Table 1). MD of 1.86% and 1.73% was obtained for 20NiAl and 30NiAl respectively.

TPR profile of 20NiOAl and 30NiOAl are shown in Fig. 2. TPR profile of calcined γ-Al_2O_3 was also evaluated to verify reducibility of γ-Al_2O_3. However, no reduction peaks were observed thereby confirming that γ-Al_2O_3 is fairly stable and absolutely non-reducible over whole range of temperatures studied. Two clearly distinguished reduction peaks were however observed for calcined catalysts. The lower temperature broad reduction peaks were

Please cite this article in press as: V. Dhanala, et al., J. Ind. Eng. Chem. (2015), http://dx.doi.org/10.1016/j.jiec.2014.12.029

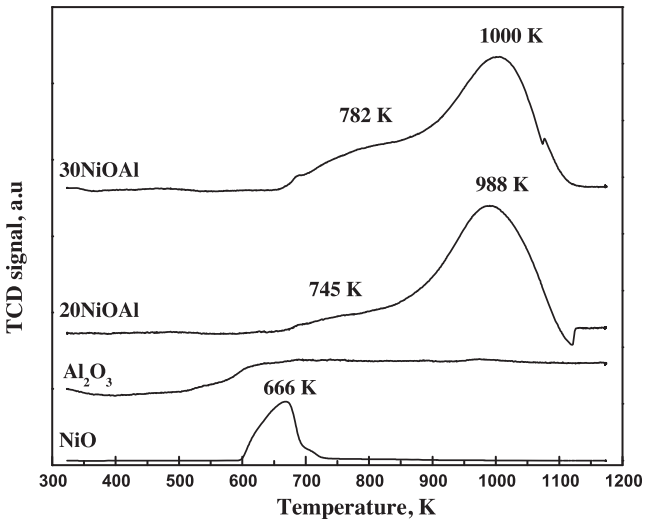

Fig. 2. TPR profiles of NiO, γ-Al_2O_3, 20NiOAl, and 30NiOAl.

observed at 745 K and 782 K for 20NiOAl and 30NiOAl respectively. To ascertain these reduction peaks, TPR profile of bulk nickel oxide was also acquired. The results clearly showed that these peaks were attributed to the reduction of bulk nickel oxide. However, these peaks were comparatively broader and shifted gradually to higher temperature with increasing nickel loadings on γ-Al_2O_3 relative to bulk nickel oxide peaks. These results undoubtedly suggested existence of weak interaction of bulk nickel oxide with γ-Al_2O_3. The shifting of reduction peak to higher temperature for higher nickel loadings on γ-Al_2O_3 may also be due to higher quantities of enlarged bulk nickel oxide crystallites. Powder XRD patterns also confirmed enlargement of nickel/nickel oxide crystallites with increasing nickel loading on γ-Al_2O_3.

Higher temperature reduction peaks were observed at 988 K and 1000 K for 20NiOAl and 30NiOAl respectively. These peaks were due to reducible dispersed $NiAl_2O_4$ spinel [28]. Powder XRD patterns also manifested $NiAl_2O_4$ peaks in 20NiOAl, 30NiOAl, and 30NiAl. In $NiAl_2O_4$ spinel, Ni^{2+} ions were incorporated non-stoichiometrically in tetrahedral (Ni_{td}) or octahedral (Ni_{oct}) sites of γ-Al_2O_3. The dispersed Ni_{td} were reduced at relatively lower temperature than dispersed Ni_{oct} [28]. The increase of nickel loading on γ-Al_2O_3 enriched reducible Ni_{oct} species leading to rise of reduction temperature [28]. The relative peaks area and intensity further suggests that majority of nickel oxide exists as dispersed $NiAl_2O_4$ form on γ-Al_2O_3.

Chemical reactions and process variables

Investigation of SR and OSR of isobutanol were carried out in a computer controlled fixed-bed reactor over γ-Al_2O_3 supported nickel catalysts under wide range of oxygen-to-carbon mole ratios (OCMR) (0.8–2.5), temperatures (773–923 K), and steam-to-carbon mole ratios (SCMR) (1.5–3.2). The H_2, CO, CO_2, and CH_4 were observed as gaseous products. The basic chemical reactions that led to formation of these gaseous products in SR and OSR are outlined in Scheme 1.

Steam reforming reaction

$$i-C_4H_{10}O + 3H_2O \leftrightarrow 4CO + 8H_2 \qquad \Delta H^o_{298K} = 558.32\ \text{kJ/mol} \qquad \text{(i)}$$

Water-gas shift reaction

$$CO + H_2O \leftrightarrow CO_2 + H_2 \qquad \Delta H^o_{298K} = -41.1\ \text{kJ/mol} \qquad \text{(ii)}$$

Overall reaction

$$i-C_4H_{10}O + 7H_2O \leftrightarrow 4CO_2 + 12H_2 \qquad \Delta H^o_{298K} = 394\ \text{kJ/mol} \qquad \text{(iii)}$$

Methanation reactions

$$CO + 3H_2 \leftrightarrow CH_4 + H_2O \qquad \Delta H^o_{298K} = -205.2\ \text{kJ/mol} \qquad \text{(iv)}$$

$$CO_2 + 4H_2 \leftrightarrow CH_4 + 2H_2O \qquad \Delta H^o_{298K} = -165\ \text{kJ/mol} \qquad \text{(v)}$$

Partial oxidation reactions

$$i-C_4H_9OH + \frac{3}{2}O_2 \leftrightarrow 4CO + 5H_2 \qquad \Delta H^o_{298K} = -160\ \text{kJ/mol} \qquad \text{(vi)}$$

Coke forming reaction

$$CH_4 \leftrightarrow C + 2H_2 \qquad \Delta H^o_{298K} = 74.9\ \text{kJ/mol} \qquad \text{(vii)}$$

$$CO + H_2 \leftrightarrow C + H_2O \qquad \Delta H^o_{298K} = -131.3\ \text{kJ/mol} \qquad \text{(viii)}$$

$$2CO \leftrightarrow C + CO_2 \qquad \Delta H^o_{298K} = 172.4\ \text{kJ/mol} \qquad \text{(ix)}$$

Scheme 1. Chemical reactions involved in oxidative steam reforming of isobutanol.

The products composition in OSR can be tuned by appropriate selection of process variables, OCMR, SCMR, and WHSV. The generalized definitions of these process variables used throughout the article are defined below. As observed from Eq. (vi) of Scheme 1, 1.5 mol of oxygen is required for complete conversion of 1 mol of isobutanol to CO and H_2. Therefore, 1.5 was considered as stoichiometric OCMR for Eq. (1). This definition of OCMR represents extents surplus or deficient oxygen supplied compared to theoretical maximum requirements of 1. One can further observe from Eq. (iii) of Scheme 1 that 7 mol of water is required for complete conversion of 1 mol of isobutanol to CO_2 and H_2. Therefore, stoichiometric SCMR of 7 was used in Eq. (2). This definition of SCMR signifies extents of excess water supplied compared to theoretical requirements of 1. In general, excess water is supplied to overcome thermodynamic limitations of water-gas shift reaction (WGSR) and reduce coke formation on the catalysts.

$$\text{Oxygen-to-carbon mole ratio} = \frac{(\text{rate of moles of oxygen}/\text{rate of moles of isobutanol})}{(\text{rate of moles of oxygen}/\text{rate of moles of isobutanol})_{stoichiometric}} = \frac{\text{rate of moles of oxygen}}{1.5 \times \text{rate of moles of isobutanol}} \quad (1)$$

$$\text{Steam-to-carbon mole ratio} = \frac{(\text{rate of moles of water fed}/\text{rate of moles of isobutanol fed})}{(\text{moles of water}/\text{moles of isobutanol})_{stoichiometric}} = \frac{\text{rate of moles of water fed}}{7 \times \text{rate of moles of isobutanol fed}} \quad (2)$$

$$\text{Weight hourly space velocity, } h^{-1} = \frac{\text{total mass flow rate of isobutanol, water, nitrogen, and oxygen}}{\text{weight of catalyst}} \quad (3)$$

The progress of OSR is generally expressed in terms of carbon conversion to gaseous products (CCGP), hydrogen yield, and selectivity to CO, CO_2, and methane. The generalized expressions of these progress variables used throughout the article are represented by following equations. As observed from Eq. (iii) of Scheme 1, maximum of 12 mol of hydrogen can be produced from 1 mol of isobutanol. However, number of moles of hydrogen produced per mole isobutanol is practically far less due to thermodynamic limitation of WGSR and incomplete reforming of methane. Therefore, stoichiometric hydrogen yield of 12 was used in Eq. (5). The present definition of hydrogen yield therefore represents how far-off actual hydrogen yields from theoretical maximum of 100%.

$$\text{Carbon conversion to gaseous products, \%} = 100 \times \frac{\text{rate of moles of carbon leaving as gaseous products}}{\text{rate of moles of carbon fed}} = 100 \times \frac{\text{rate of moles of CO, } CO_2\text{, and } CH_4 \text{ formed}}{4 \times \text{rate of moles of isobutanol fed}} \quad (4)$$

$$\text{Hydrogen yield, \%} = 100 \times \frac{\left(\text{rate of moles of hydrogen formed}/\text{rate of moles of isobutanol fed} \times \text{fractional CCGP}\right)}{\left(\text{rate of moles of hydrogen formed}/\text{rate of moles of isobutanol reacted}\right)_{stoichiometric}} = 100 \times \frac{\text{rate of moles of hydrogen formed}}{12 \times \text{rate of moles of isobutanol fed} \times \text{fractional CCGP}} \quad (5)$$

$$\text{Selectivity to CO, } CO_2\text{, or } CH_4\text{, \%} = 100 \times \frac{\text{rate of moles of CO, } CO_2\text{, or } CH_4 \text{ formed}}{\text{rate of moles of CO} + CO_2 + CH_4 \text{ formed}} \quad (6)$$

The acetaldehyde, propionaldehyde, isobutyraldehyde, 2-propenal, 2-butanone, 1-butanol, 2-butanol, and unreacted isobutanol were identified as products in liquid samples. The carbon balance was checked for all experiments and errors were within ±10% (Table 2). As observed from table, unreacted butanols were major products in liquid sample in all experiments. It was further observed that molar flow rates of products in liquid samples were decreased with increasing OCMR, temperature, and SCMR. However, these products were excluded from selectivity calculations for better comparisons with equilibrium selectivity to CO, CO_2, and methane. The reproducibility of the experiments was also checked for few runs as shown in Table 2. The molar flow rates of various products were matched closely for repeated runs thereby confirming that experimental data are reasonably reproducible. Moreover, the activity of pure γ-Al_2O_3 was also examined for SR and OSR and negligible CCGP was observed under the experimental conditions thereby demonstrating that γ-Al_2O_3 alone played insignificant role for SR and OSR.

Time-on-stream behaviour of 30NiAl for OSR

The catalysts stability of 30NiAl for OSR was verified for about 12 h of TOS (Fig. 3). 100% CCGP was persisted over entire range of TOS. The product gas composition reached to steady state within first 2 h of TOS. After initial 2 h of TOS, the hydrogen yield and selectivity to CO, CO_2, and methane were remained practically consistent up to 12 h of TOS. These results confirmed that γ-Al_2O_3 supported nickel catalysts were fairly stable under the experimental conditions. All subsequent experiments were conducted for minimum of 4 h of TOS. The products composition data were collected after 2 h of TOS for all experiments.

Effects of oxygen-to-carbon mole ratio

The effects of OCMR were investigated experimentally at 873 K with SCMR of 2.5 (Fig. 4). The experiments were performed at various oxygen flow rates in the feed equivalent to OCMR in the range of 0–2.5 keeping all other process parameters constant. The experiments were designed well below OCMR of 4 to avoid complete combustion of isobutanol to CO_2 and H_2O. The introduction of oxygen in the feed however resulted slightly increasing trends of WHSV with increasing OCMR. In the product gas, even traces of oxygen was not detected in any of the experiments thereby confirming that oxygen completely reacted with isobutanol, intermediate compounds, or products within the reactor. The CCGP was increased from ~89% to ~98% with increasing OCMR from 0 to 2.5. The increase of CCGP was mainly due to enhanced oxidation of isobutanol or intermediate compounds with increasing OCMR. The hydrogen yield and selectivity to CO and CH_4 was however reduced and selectivity to CO_2 was increased continually with increasing OCMR. The hydrogen yield was reduced to just 30% from 73%, while selectivity to CH_4 was dropped to only 0.3% from 13.5% with increase of OCMR from 0 to 2.5. These results suggested that oxidation of hydrogen, CO, and CH_4 into H_2O and CO_2 was promoted with increasing levels of oxygen in the feed thereby decreasing hydrogen yield and selectivity to CO and CH_4. Identical trends were also reported earlier for OSR of ethanol [29]. The equilibrium products compositions were also calculated under identical experimental conditions at three different temperatures and compared with experimental hydrogen yield and

Please cite this article in press as: V. Dhanala, et al., J. Ind. Eng. Chem. (2015), http://dx.doi.org/10.1016/j.jiec.2014.12.029

Table 2
Carbon balance table for SR and OSR of isobutanol.

	Gas products flow rates (mol h^{-1})				Liquid products flow rates $\times 10^5$ (mol h^{-1})						CBE
	H_2	CO	CH_4	CO_2	ACE	PPD	PPL	BUD	BUN	BU	
OCMR	*Effects of OCMR for OSR*[a]										
0	0.406	0.052	0.025	0.107	1.3	2.67	2	0.32	3.1	90.5	9.6
0.8	0.363	0.043	0.005	0.137	2.83	50.7	27.6	0.14	32.3	70.4	7.9
1.7	0.318	0.040	0.003	0.147	2.06	34.7	16	0	17.9	8.5	7.4
2.5	0.183	0.023	0.001	0.179	2.3	26.42	6.65	0	11.92	2.96	1.6
Temperature (K)	*Effects of temperature for SR*[b]										
773	0.277	0.027	0.04	0.117	2.81	3.04	3	0	4.26	78.3	9.8
823	0.311	0.036	0.033	0.13	0.65	2.02	0	0	2.31	38.1	3.5
873	0.455	0.044	0.03	0.133	0.278	0.56	0	0	0.79	0.22	0.45
923	0.499	0.060	0.011	0.137	0	0.12	0	0.164	0.178	0.179	−0.01
Temperature (K)	*Effects of temperature for OSR*[c]										
773	0.236	0.019	0.027	0.136	1.67	63.5	25.7	0	28	65	9.4
823	0.308	0.026	0.022	0.138	0.57	16.07	7.1	0	6.5	46	9.2
873^{R1}	0.394	0.043	0.012	0.146	0.16	2.5	0.63	0	1.5	1.3	3.2
873^{R1}	0.376	0.04	0.017	0.140	0.4	10.62	2.62	0	1.9	37.2	4.3
923^{R2}	0.42	0.06	0.004	0.142	0.025	0.52	0.15	0	0.38	0.7	1.4
923^{R2}	0.45	0.06	0.004	0.142	0.789	1.3	0.50	0	0.27	2.5	1.1
SCMR	*Effects of SCMR for SR*[d]										
1.5	0.593	0.140	0.035	0.104	0.072	1.3	1	0	1.51	3.211	1.67
2	0.504	0.081	0.02	0.115	0.048	1.63	0	0.046	0.303	3.52	6.8
2.5	0.499	0.060	0.011	0.137	0	0.12	0	0.164	0.178	0.179	−0.01
3.2	0.424	0.049	0.004	0.103	0.06	0.02	0	0	0	0.07	−2.63
SCMR	*Effects of SCMR for OSR*[e]										
1.5	0.493	0.098	0.018	0.155	3.3	2.17	50.13	0	0.69	5.95	4
2	0.439	0.077	0.01	0.146	2.06	6.05	57.87	0	0.87	27.81	−1.7
2.5	0.448	0.059	0.005	0.142	0.79	1.31	0.501	0	0.27	2.54	0.9
3.2	0.32	0.033	0.001	0.121	0.22	0.069	122.8	0	0.35	0.36	−4.4

ACE, acetaldehyde; PPD, propionaldehyde; PPL, 2-propenal; BUD, butyraldehyde; BUN, 2-butanone; BU, 1-, 2-, and iso-butanol; CBE, carbon balance error, %.
[a] Isobutanol = 0.052 mol h^{-1}, H_2O = 0.9 mol h^{-1}, and N_2 = 0.14 mol h^{-1}. Conditions: 20NiAl, 873 K, SCMR = 2.5, WHSV = 7.02, 7.6, 8.3 and 8.9 h^{-1} for OCMR of 0.8, 1.7 and 2.5 respectively.
[b] Isobutanol = 0.052 mol h^{-1}, H_2O = 0.9 mol h^{-1}, and N_2 = 0.14 mol h^{-1}. Conditions: 30NiAl, SCMR = 2.5, WHSV = 7.02 h^{-1}.
[c] Isobutanol = 0.052 mol h^{-1}, H_2O = 0.9 mol h^{-1}, and N_2 = 0.14 mol h^{-1}. Conditions: 30NiAl, SCMR = 2.5, OCMR = 0.8, WHSV = 7.6 h^{-1}.
[d] Isobutanol = 0.071, 0.058, 0.052, and 0.038 mol h^{-1} and H_2O = 0.73, 0.8, 0.9, and 0.87 mol h^{-1} for SCMR of 1.5, 2, 2.5, and 3.2 respectively, and N_2 = 0.14 mol h^{-1}. Conditions: 30NiAl, 923 K, WHSV = 6.5 h^{-1}.
[e] Isobutanol = 0.071, 0.058, 0.052, and 0.038 mol h^{-1} and H_2O = 0.73, 0.8, 0.9, and 0.87 mol h^{-1} for SCMR of 1.5, 2, 2.5, and 3.2 respectively, and N_2 = 0.14 mol h^{-1}. Conditions: 30NiAl, 923 K, OCMR = 0.8, WHSV = 7.6 h^{-1}.
[R1, R2] Reproducibility results.

selectivity to CO_2 and CH_4 as presented in Fig. 4. As observed from the figure, experimental trends of hydrogen yield and selectivity to CO_2 and CH_4 were fully consistent with thermodynamic equilibrium analysis results.

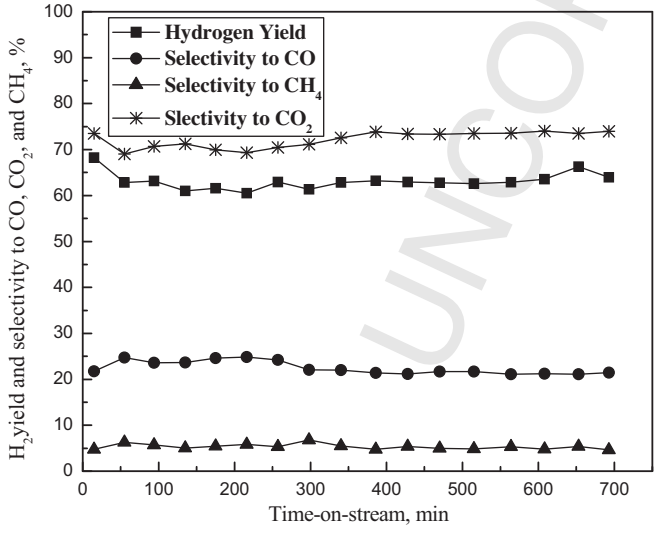

Fig. 3. Time-on-stream behaviour of 30NiAl catalyst for OSR. Experimental conditions: 873 K, SCMR = 2.5, WHSV = 7.6 h^{-1}, OCMR = 0.8, CCGP = 100%.

Thermoneutral conditions

The principal advantage of OSR is that heat required for endothermic SR reactions can be generated in situ by exothermic PO reactions. Therefore, maintaining appropriate OCMR depending on process conditions is crucial to accomplish thermoneutral

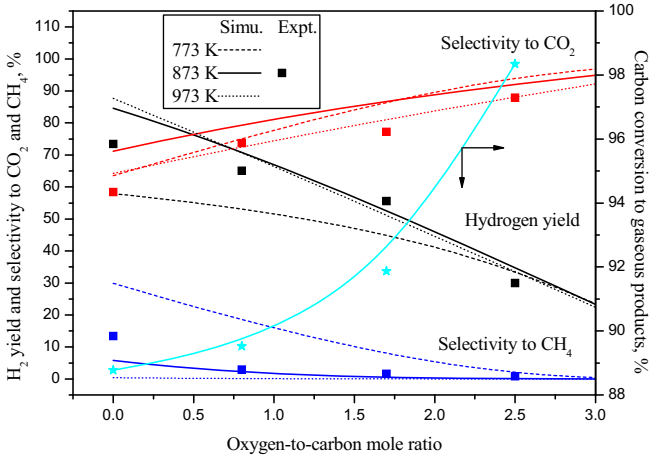

Fig. 4. Effects of oxygen-to-carbon mole ratio on hydrogen yield, and selectivity to CO_2 and CH_4 for OSR. Experimental conditions: 20NiAl, 873 K, SCMR = 2.5, WHSV = 7.02, 7.6, 8.3 and 8.9 h^{-1}.

operation (condition at which heat duty = 0). The heat duty of the process governs mainly by feed and reactor temperature and OCMR. In the present study, heat duty analysis was performed considering feed (consisting of isobutanol, water, and oxygen) entered at reactor temperature. As observed from Fig. 5A, the process becomes increasingly exothermic with increasing OCMR for a fixed temperature. However, for fixed OCMR, process become increasingly endothermic with increasing temperature. As noted from the figure, OCMR of 0.5, 0.6, and 0.7 are necessary for thermoneutral operation at 808 K, 854 K, and 1075 K respectively. The equilibrium SG composition at thermoneutral conditions is shown in Fig. 5B. As observed from the figure, selectivity to methane is decreasing with increasing temperature and it is almost negligible at 1075 K with OCMR = 0.7. The selectivity of CO was increasing with increasing temperature.

Effects of temperature

The experimental investigations of SR of isobutanol were conducted in the temperatures range of 773–923 K with SCMR of 2.5 and WHSV of 7.02 h^{-1} as shown in Fig. 6A. As observed from the figure, CCGP was increased with increasing temperature. The CCGP was just ~89% at 773 K and reached to 100% at 923 K. The increase of CCGP was mainly due to enhancements of endothermic SR reactions (Eq. (i) and reverse of Eqs. (iv) and (v) of Scheme 1) at elevated temperatures. The equilibrium calculations were however performed in the temperature range of 623–1173 K at three different SCMRs, 1.5, 2.5, and 3.5. The equilibrium results were then compared with experimental hydrogen yield and selectivity

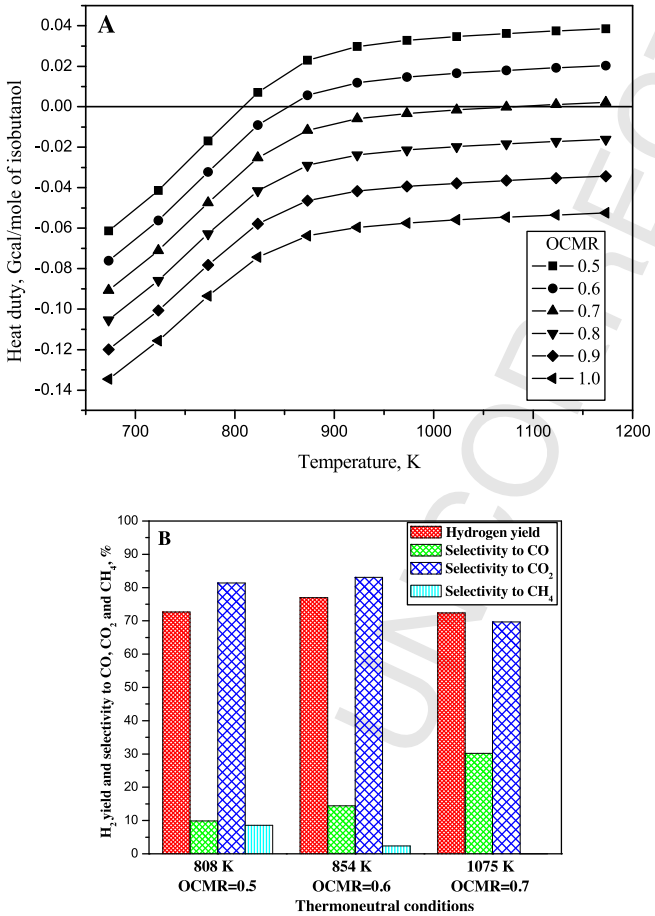

Fig. 5. A. Heat duty analysis for OSR of isobutnaol and B. equilibrium composition of synthesis gas at thermoneutral conditions with SCMR = 3.2.

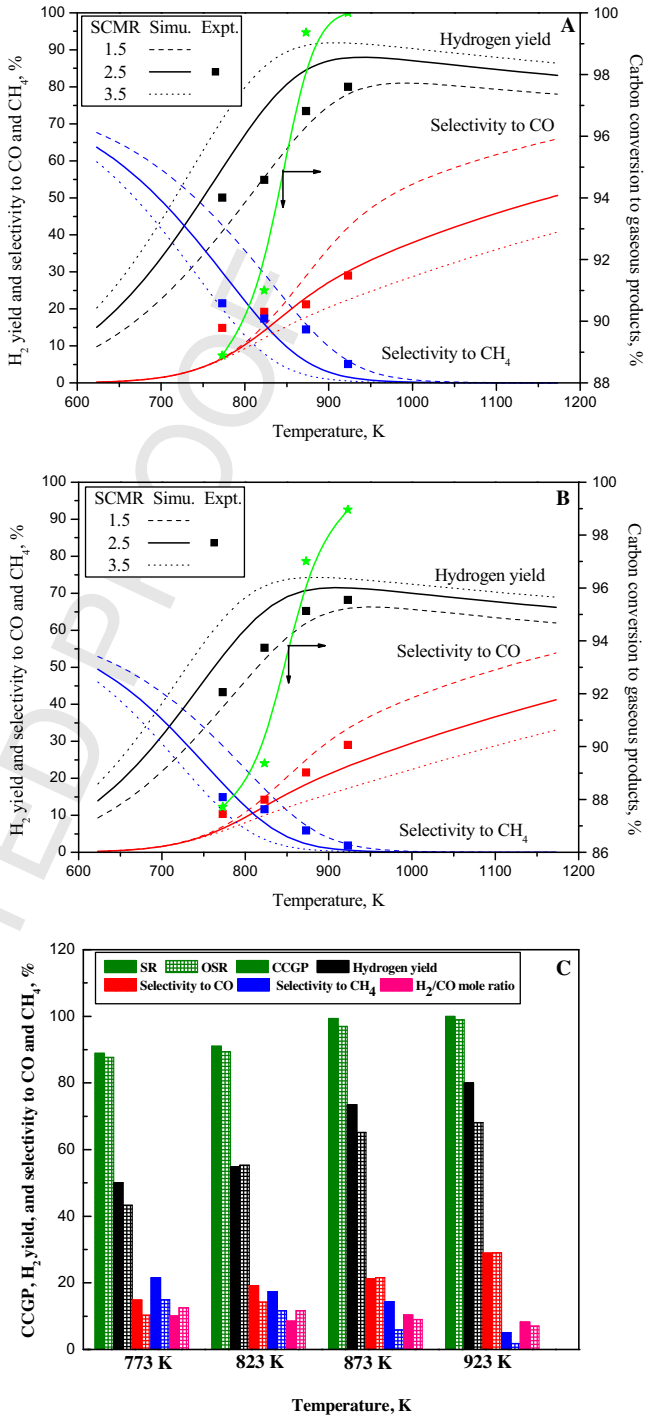

Fig. 6. Effects of temperature on CCGP, hydrogen yield, and selectivity to CO and CH_4 for (A) SR, (B) OSR, and (C) comparison of SR and OSR of isobutanol. Experimental conditions: 30NiAl, SCMR = 2.5. WHSV = 7.02 h^{-1} (SR) and 7.6 h^{-1} (OSR).

to CO and CH_4 (Fig. 6A). As observed from the figure, equilibrium results were fully consistent with experimental data.

For fixed SCMR, equilibrium hydrogen yield was increased sharply with increasing temperature and reached a maximum at about 903–969 K depending on SCMR. The hydrogen yield was then started declining slowly with further increase of temperatures. The maximum experimental hydrogen yield of ~80% was observed at 923 K and SCMR of 2.5 compared to theoretical maximum of ~87%. The slightly lesser experimental hydrogen yield clearly indicates that reactions are somewhat away from the

equilibrium. On the other hand, selectivity to CO was increased and selectivity to CH_4 was dropped with increasing temperature. The experimental selectivity to CH_4 was reduced to only 5% at 923 K with SCMR of 2.5. These observations can be explained by the fact that endothermic SR reactions (Eq. (i) and reverse of Eqs. (iv) and (v) of Scheme 1) are favourable at elevated temperature; while exothermic WGSR (Eq. (ii) of Scheme 1) are favoured at lower temperature. At relatively lower temperature (below temperature of maximum of hydrogen yield) with high concentration of methane, contribution of endothermic SR reactions on hydrogen yield were dominating over exothermic WGSR leading to growing trends of hydrogen yield with increasing temperature. However, at sufficiently high temperatures with very low concentration of methane, SR of methane became unimportant and exothermic WGSR became sole contributing factor on hydrogen yield leading to slightly declining trends of hydrogen yield with increasing temperatures. It was further observed from the figure that temperatures of maximum hydrogen yield were moved gradually to lower temperature with increasing SCMR. This was due to the fact that selectivity to methane was reached to low value at relatively lesser temperature at higher SCMR.

The effects of temperature on OSR of isobutanol were investigated at OCMR of 0.8 under otherwise identical experimental conditions of SR. The thermodynamic equilibrium analysis of OSR of isobutanol was carried out at SCMRs of 1.5, 2.5, and 3.5. The equilibrium results were then compared with experimental data as shown in Fig. 6B. Fairly decent agreements were also observed between equilibrium and experimental hydrogen yield and selectivity to CO and CH_4. As observed from the figure, the trends of OSR results were fully analogous to SR. Hence, similar arguments can be used to explain trends of OSR results as well.

The comparisons of experimental OSR results with SR are presented in Fig. 6C. As shown in figure, CCGP was somewhat lesser for OSR compared to SR. The molar flow rates of products in liquid samples were also slightly higher in OSR than SR (Table 2). The lesser CCGP and higher levels of products in liquid samples in OSR were mainly due to slightly higher WHSV compared to SR (owing to added oxygen flow in feed for OSR). The hydrogen yield and selectivity to CO and CH_4 were however lesser for OSR compared to SR. Experimental hydrogen yield was only ~68% for OSR compared to ~80% for SR at 923 K. The selectivity to CH_4 was dropped to below 2% for OSR from ~5% for SR at 923 K. Such a low selectivity to methane is one of the biggest advantages of OSR. These results clearly indicated that hydrogen, CO, and methane were oxidized by oxygen leading to drop in hydrogen yield and selectivity to CO and methane for OSR compared to SR [30,31]. Thermodynamic equilibrium analysis results further revealed that temperatures corresponding to maximum hydrogen yield were somewhat lesser for OSR (864–932 K) compared to SR (903–969 K). This was mainly due to lesser selectivity to methane OSR compared to SR for a fixed temperature and SCMR.

The requirements of H_2/CO mole ratio generally vary depending upon downstream applications of SG. For example, H_2/CO mole ratio in the range of 1.7–2.15 is required for Fisher–Tropsch synthesis of methanol, dimethyl ether, and hydrocarbons. As seen from Fig. 6C, H_2/CO mole ratio remained practically unaffected by temperature for both SR and OSR. With increasing temperature, both hydrogen yield and selectivity to CO was increased thereby keeping H_2/CO mole ratios almost unchanged. It was further observed from the figure, H_2/CO mole ratios were virtually same for both SR and OSR. These results clearly demonstrated that hydrogen and CO were equally oxidized in presence of oxygen thereby maintaining consistent H_2/CO mole ratios for both SR and OSR. In the present study, H_2/CO mole ratios in the range of 8–10 were observed for both SR and OSR under the experimental conditions.

Effects of steam-to-carbon mole ratio

The SR experiments were conducted over 30NiAl at 923 K and 6.5 h^{-1} WHSV in the SCMR range of 1.5–3.2 as illustrated in Fig. 7A. For accurate comparisons of results, WHSV for all experiments was kept constant by maintaining same total mass flow rate of feed (with different mole ratios of isobutanol and water) and weights of the catalyst (Table 2). Almost complete CCGP was observed for

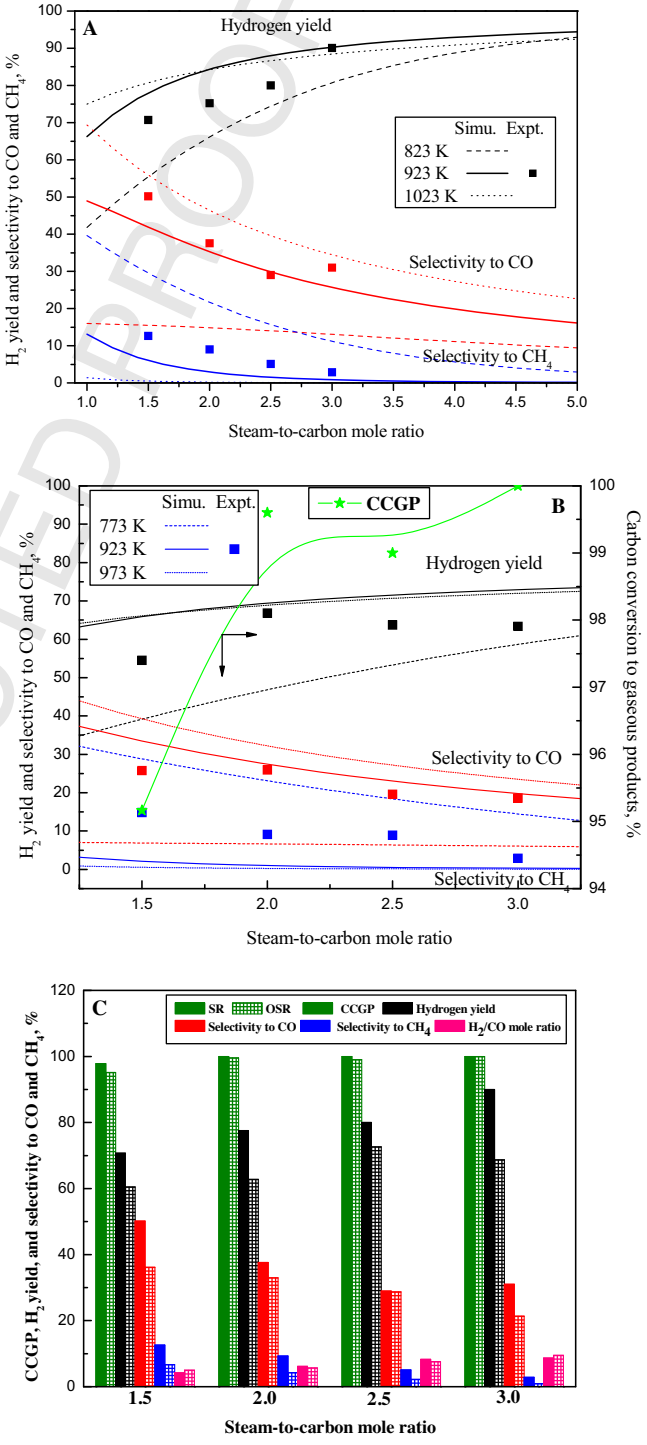

Fig. 7. Effects of steam-to-carbon mole ratio on hydrogen yield and selectivity to CO and CH_4 for (A) SR, (B) OSR, and (C) comparison of SR and OSR of isobutanol. Experimental conditions: 30NiAl, 923 K. WHSV = 6.5 h^{-1} (SR) and 7.6 h^{-1} (OSR), CCGP = 100% (SR), OCMR = 0.8.

whole ranges of SCMR studied. Thermodynamic equilibrium analysis was performed at three different temperatures (823, 923, and 1023 K) under otherwise identical experimental conditions. The equilibrium results were agreed reasonably well with experimental hydrogen yield and selectivity to CO and CH_4 as shown in the figure.

The hydrogen yield was increased with increasing SCMR for a fixed temperature. The selectivity to CO and CH_4 was however decreased with increasing SCMR. The maximum of 90% hydrogen yield with less than 3% selectivity to CH_4 was observed experimentally at SCMR of 3.2. With increase of SCMR, SR of isobutanol, SR of methane (reverse of Eqs. (iv) and (v) of Scheme 1), and WGSR (Eq. (ii) of Scheme 1) were favoured thereby increasing hydrogen yield and decreasing selectivity to CO and CH_4. Similar trends of experimental and equilibrium results were also reported earlier for SR of aqueous phase of bio-oil [32].

Effects of SCMR on OSR of isobutanol were also examined at OCMR of 0.8 and WHSV of 7.6 h^{-1} under otherwise identical

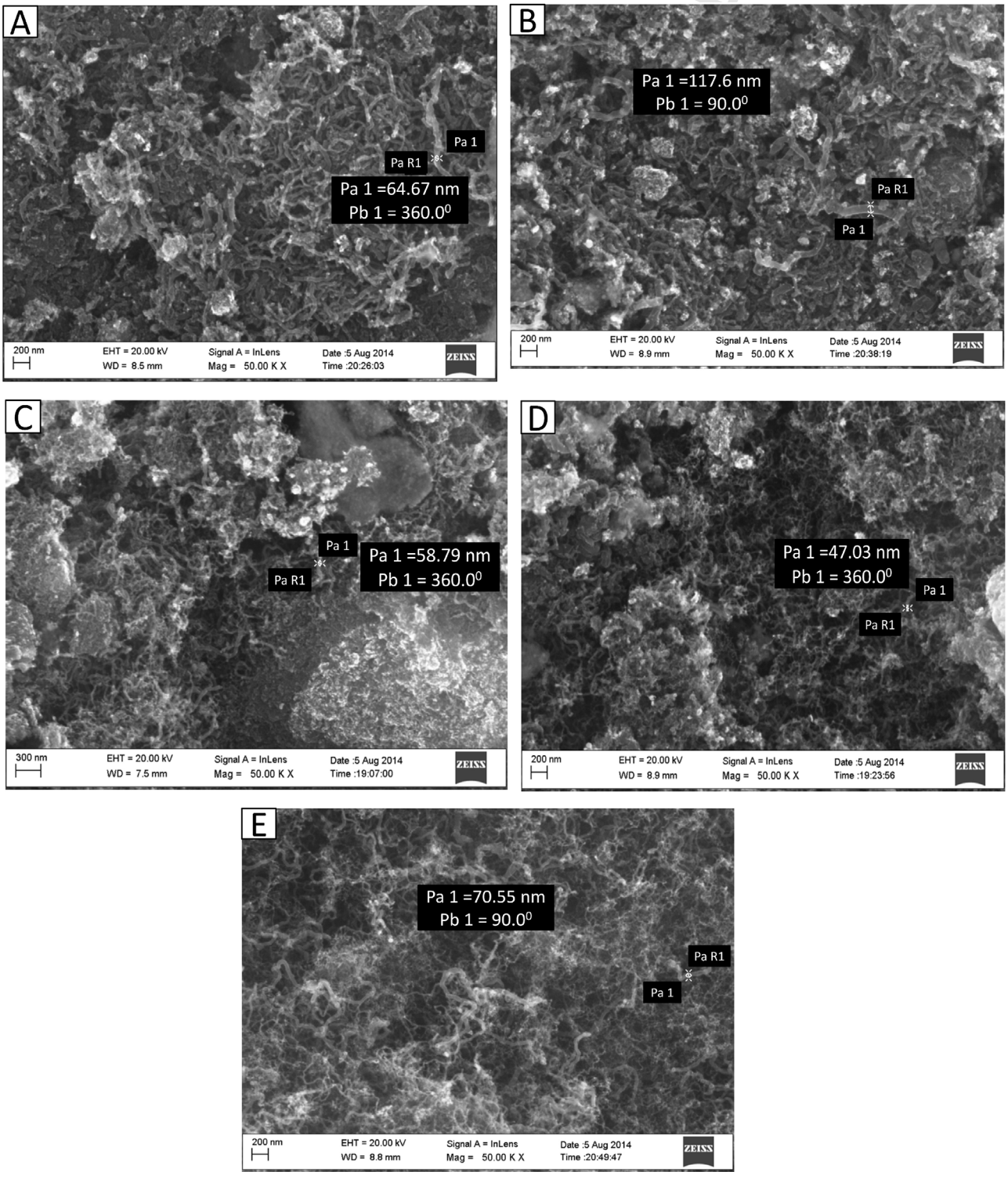

Fig. 8. SEM images of spent catalysts. (A) 20NiAl (SR), (B) 30NiAl (SR), (C) 20NiAl with OCMR = 0.8, (D) 20NiAl with OCMR = 1.7 and (E) 30NiAl with OCMR = 0.8.

Please cite this article in press as: V. Dhanala, et al., J. Ind. Eng. Chem. (2015), http://dx.doi.org/10.1016/j.jiec.2014.12.029

experimental condition of SR as shown in Fig. 7B. As shown in the figure, CCGP was increased with increasing SCMR. The CCGP was about 95% at SCMR of 1.5 and touched 100% at SCMR of 3.2. The equilibrium calculations for OSR of isobutanol were also carried out at three different temperatures, 823, 923, and 1023 K. The experimental OSR results matched reasonably well with equilibrium predictions. Moreover, identical trends of results were also observed for both SR and OSR. Therefore, arguments used for explanation of trends of SR results are equally applicable for OSR.

The comparisons of experimental SR and OSR results are shown in Fig. 7C. As observed, CCGP was slightly higher for SR than OSR. The molar flow rate of products in liquid sample was somewhat more in OSR compared to SR (Table 2). This was mainly due to incomplete CCGP because of slightly higher WHSV for OSR than SR. However, hydrogen yield and selectivity to CO and CH_4 were lesser for OSR compared to SR as observed from Fig. 7C. This result indicates that hydrogen, CO, and CH_4 were oxidized by oxygen to water and CO_2 thereby reducing hydrogen yield and selectivity to CO and CH_4. As observed from the figure, H_2/CO mole ratio was enhanced with increasing SCMR. The H_2/CO mole ratio was below 5 at SCMR of 1.5 and increased to 10 at SCMR of 3.2. This was mainly because of the fact that hydrogen yield was increased and selectivity to CO was decreased with increasing SCMR thereby increasing H_2/CO mole ratio. However, H_2/CO mole ratio remained almost same for both SR and OSR.

Spent catalysts characterization

Powder XRD

Spent catalysts were characterized by powder XRD to understand role of OCMR on chemical changes of supported nickel catalysts during SR and OSR (Fig. 1). Powder XRD patterns of spent catalysts showed characteristic peaks of nickel (44.5°, 51.97°, 76.47°, and 92.6°), nickel oxide (37.37°, 43.2° and 50.85°), and $NiAl_2O_4$ (37.37° and 66.2°) depending on OCMR. For SR, excepting combined peak at 2θ of 37.3° for nickel/nickel oxide, spent 20NiAl showed representative peaks of nickel only. The existence of bulk nickel oxide on spent 20NiAl during SR thus remained inconclusive. Interestingly, with increasing OCMR, nickel oxide peaks were appeared gradually with concurrent decrease of intensity of nickel peaks. At OCMR = 2.5, only nickel oxide and $NiAl_2O_4$ peaks were observed in spent 20NiAl. Moreover, intensity of one signature $NiAl_2O_4$ peak at 2θ of ~66.2° was decreased gradually with increasing OCMR for spent 20NiAl. These results clearly endorsed that nickel and $NiAl_2O_4$ converted to bulk nickel oxide during OSR. For spent 20NiAl, average nickel crystallite size was decreased from 15.3 nm to 8.2 nm with increasing OCMR from 0 to 1.7 (Table 1). However, average nickel/nickel oxide crystallite sizes were remained practically unaffected with increasing OCMR for 30NiAl. The nickel oxide crystallites were however enlarged in spent catalysts of SR and OSR compared to fresh calcined catalysts.

SEM analysis

FESEM images of selected spent catalysts are presented in Fig. 8. The EDX spectrums of the spent catalysts are shown as supplementary information (Fig. S1). A complex criss-cross carbon nano-fibres networks were formed on spent γ-Al_2O_3 supported nickel catalysts for both SR and OSR. These carbon nano-fibres were formed on active metals by decomposition of carbonaceous compounds (Eqs. (vii)–(ix) of Scheme 1) [33]. The carbon nano-fibres networks were denser and bigger in diameter over spent 30NiAl than spent 20NiAl for both SR and OSR. These results clearly suggested that extents and diameter of carbon nano-fibres increased with increasing nickel crystallite size [34]. Some researchers however reported that diameter of carbon nano-fibres was independent of initial nickel crystallite size and depends mainly on structural transformations during carbon growth process [35,36]. The density of carbon nano-fibres and their diameter were however lesser for OSR compared to SR. The diameter of carbon nano-fibres was decreased to 70.5 nm for OSR at 0.8 OCMR from 117.6 nm for SR for spent 30NiAl. For spent 20NiAl, diameter of carbon nano-fibres was 64.7 nm for SR and decreased to 58.8 nm for OSR at 0.8 OCMR. The diameter of carbon nano-fibres was further decreased with increasing OCMR. For OSR over 20NiAl, diameter of carbon nano-fibres was decreased from 58.8 nm to 47 nm for increasing OCMR from 0.8 to 1.7. The decrease of diameter of carbon nano-fibres may be due to increased oxidation of carbon deposited on the catalysts at elevated OCMR.

Supplementary Fig. 1 can be found, in the online version, at doi:10.1016/j.jiec.2014.12.029.

Conclusions

The current work presents a comprehensive investigation of SR and OSR of isobutanol over γ-Al_2O_3 supported nickel catalysts in a computer controlled fixed-bed reactor. The experimental results were further authenticated with equilibrium products composition. The experimental data were matched well with thermodynamic equilibrium analysis results. The catalysts characterization results suggested that majority of nickel oxide was present as dispersed $NiAl_2O_4$ on γ-Al_2O_3. The rise of OCMR led to decline of hydrogen yield and selectivity to CO and methane. The hydrogen yield was dropped to 68% from 80%; while selectivity to methane was reduced to 1.7% from 4.8% with increasing OCMR from 0 to 2.5 at 923 K and SCMR of 2.5. The hydrogen yield and selectivity to CO was increased with concurrent decrease of selectivity to methane with rise of temperature for both SR and OSR. With increasing SCMR, hydrogen yield was boosted and selectivity to CO and methane was reduced for both SR and OSR. The H_2/CO mole ratio was consistent for both SR and OSR and enhanced with increasing SCMR. The H_2/CO mole ratio of 7–8 was obtained at 923 K and SCMR of 2.5. The powder XRD patterns of spent catalysts exhibited oxidation of nickel to nickel oxide during OSR. The FESEM images of spent catalysts showed that diameter of carbon nano- fibres were reduced with increasing OCMR.

References

[1] S. Fernando, S. Adhikari, C. Chandrapal, N. Murali, Energy Fuels 20 (2006) 1727.
[2] S.K. Maity, Renew. Sustain. Energy Rev. (2014), http://dx.doi.org/10.1016/j.rser.2014.08.075i.
[3] T.A. Milne, R.J. Evans, N. Abatzoglu, NREL, 1998 Available from: http://www.nrel.gov/docs/fy99osti/.
[4] A. Haryanto, S. Fernando, N. Murali, S. Adhikari, Energy Fuels 19 (2005) 2098.
[5] M. Ni, D.Y.C. Leung, M.K.H. Leung, Int. J. Hydrogen Energy 32 (2007) 3238.
[6] A.S. Chattanathan, S. Adhikari, N. Abdoulmoumine, Renew. Sustain. Energy Rev. 16 (2012) 2366.
[7] M. Kumar, K. Gayen, Appl. Energy 88 (2011) 1999.
[8] B.-Q. He, M.-B. Liu, J. Yuan, H. Zhao, Fuel 108 (2013) 668.
[9] M. Mascal, Bio. Prod. Biorefin. 6 (2012) 483.
[10] S. Golunski, Energy Environ. Sci. 3 (2010) 1918.
[11] F. Bimbela, D. Chen, J. Ruiz, L. García, J. Arauzo, Appl. Catal. B: Environ. 119–120 (2012) 1.
[12] W. Cai, P.R. de la Piscina, N. Homs, Bioresour. Technol. 107 (2012) 482.
[13] V. Dhanala, S.K. Maity, D. Shee, RSC Adv. 3 (2013) 24521.
[14] B. Roy, H. Sullivan, C.A. Leclerc, J. Power Sources 267 (2014) 280.
[15] I.C. Lee, J.G. St. Clair, A.S. Gamson, Int. J. Hydrogen Energy 37 (2012) 1399.
[16] R. Chakrabarti, J.S. Kruger, R.J. Hermann, L.D. Schmidt, RSC Adv. 2 (2012) 2527.
[17] W. Cai, N. Homs, P.R. de la Piscina, Green Chem. 14 (2012) 1035.
[18] W. Cai, P.R. de la Piscina, K. Gabrowska, N. Homs, Bioresour. Technol. 128 (2013) 467.
[19] W. Cai, P.R. de la Piscina, N. Homs, Appl. Catal. B: Environ. 145 (2014) 56.
[20] W. Cai, N. Homs, P.R. de la Piscina, Appl. Catal. B: Environ. 150–151 (2014) 47.
[21] G.A. Nahar, S.S. Madhani, Int. J. Hydrogen Energy 35 (2010) 98.
[22] W. Wang, Y. Cao, Int. J. Hydrogen Energy 35 (2010) 13280.
[23] W. Wang, Fuel 90 (2011) 1681.
[24] A.L. da Silva, I.L. Müller, Int. J. Hydrogen Energy 36 (2011) 2057.

[25] W. Wang, Y. Cao, Int. J. Hydrogen Energy 36 (2011) 2887.
[26] S.R. Yenumala, S.K. Maity, Int. J. Hydrogen Energy 36 (2011) 11666.
[27] S.R. Yenumala, S.K. Maity, J. Renew. Sustain. Energy 4 (2012) 043120.
[28] J.G. Seo, M.H. Youn, Y. Bang, I.K. Song, Int. J. Hydrogen Energy 35 (2010) 12174.
[29] P. Biswas, D. Kunzru, Chem. Eng. J. 136 (2008) 41.
[30] N.R. Peela, D. Kunzru, Int. J. Hydrogen Energy 36 (2011) 3384.
[31] N. Srisiriwat, S. Therdthianwong, A. Therdthianwong, Int. J. Hydrogen Energy 34 (2009) 2224.
[32] P.N. Kechagiopoulos, S.S. Voutetakis, A.A. Lemonidou, I.A. Vasalos, Energy Fuels 20 (2006) 2155.
[33] M.L. Toebes, J.H. Bitter, A. Jos Van Dillen, K.P. de Jong, Catal. Today 76 (2002) 33.
[34] M.A. Nieva, M.M. Villaverde, A. Monzón, T.F. Garetto, A.J. Marchi, Chem. Eng. J. 235 (2014) 158.
[35] N. Jeong, J. Lee, J. Catal. 260 (2008) 217.
[36] C. Pham-Huu, R. Vieira, B. Louis, A. Carvalho, J. Amadou, T. Dintzer, M.J. Ledoux, J. Catal. 240 (2006) 194.

Please cite this article in press as: V. Dhanala, et al., J. Ind. Eng. Chem. (2015), http://dx.doi.org/10.1016/j.jiec.2014.12.029